Competitive Self-Assembly Kinetics as a Route to Controlling the Morphology of Core-Crystalline Cylindrical Micelles

Jiangping Xu,[1, †] Hang Zhou,[1, †] Qing Yu,[1] Ian Manners,[2,] and Mitchell A. Winnik[1, *]

[1] Department of Chemistry, University of Toronto, 80 St. George Street, Toronto, ON, M5S 1H6

[2] School of Chemistry, University of Bristol, Bristol UK, BS8 1TS

† These authors contributed equally to this work

ABSTRACT

Nucleated self-assembly in selective solvents of core-crystalline block copolymers (BCPs) is a special case of living supramolecular polymerization, leading to rod-like micelles of controlled and uniform length. For the crystallization-driven self-assembly of PFS-containing BCPs (PFS = polyferrocenyldimethylsilane), the formation of block comicelles by sequential addition of different BCPs is well established. But there are only a few examples of living copolymerization, the simultaneous addition of pairs of BCPs with different corona-forming chains. At present, relatively little is known about the competitive kinetics of different BCPs crystallizing on a common seed. Here we report a systematic study of competitive seeded growth kinetics of pairs of linear PFS-containing BCPs and show that one can manipulate the kinetics to control the morphology of the comicelles. We found that the seeded-growth kinetics of the individual BCP unimer dominates the co-assembly behavior and thus the morphology of the corona. Patchy comicelles with microphase-segregated corona chains are formed when the epitaxial growth rates of the two different BCPs on the common seed are similar. In contrast, factors that lead to dissimilar growth rates (long corona-forming blocks or introduction of charges on

corona-forming chains) promote large-scale separation of the corona blocks, leading to block comicelles. Because the termini of the comicelles remain living, they can further direct the growth of unimers, resulting in hierarchical block comicelles with patchy blocks and single-component (homo) blocks. Furthermore, the patchy comicelles can be loaded with either gold or platinum nanoparticles, generating organic-inorganic hybrid materials with potential application in catalysis.

1. INTRODUCTION

Supramolecular polymers are defined as a "polymeric array of unimers that are held together by highly directional and reversible noncovalent interactions".[1-3] This topic has attracted broad interest in the fields of polymer and material science.[4-7] A variety of non-covalent interactions have been employed to construct supramolecular polymers.[8-17] One major issue is how to realize "living" supramolecular polymerization to prepare supramolecular polymers with a very narrow length distribution.[18-22] The key problem is to inhibit spontaneous polymerization through kinetic control under the conditions of cooperative growth.[1,22] To this end, Sugiyasu, Takeuchi, and co-workers discovered a living supramolecular polymerization of porphyrin-based monomers initiated upon addition of supramolecular seeds. In their system, the monomers in solution spontaneously formed small colloidal J-aggregates that rearranged in the presence of H-aggregates to form long fiber-like structures. They found that the reaction kinetics in this system were analogous to that of conventional living chain polymerization.[22] Miyajima, Aida and coworkers developed the concept of a "meta-stable" monomer, which is conformationally restricted from step-growth polymerization, but undergoes chain-growth polymerization with living characteristics upon addition of rationally designed initiators.[19]

The formation of protein fibers in biological systems has been considered as a type of supramolecular polymerization in which the unimers that polymerize are themselves polymers. For example, amyloid fibers grow by protein deposition at both ends of seed fragments, and actin filaments grow and shrink by attachment and detachment of G-actin monomers at the two filament ends.[23] In contrast, in tubulin polymerization, protein unimers deposit on a single growing terminus.[24] Thus non-covalent polymerization in these biological systems can exhibit either unidirectional or bidirectional growth.

Another kind of non-covalent polymerization of macromolecular unimers occurs in selective solvents with block copolymers (BCPs) with a long corona-forming block and a shorter crystallizable core-forming block. Microphase separation of the core-forming block can lead to elongated fiber-like micelles via a process referred to as crystallization-driven self-assembly

(CDSA).[25-38] This is a nucleated growth process. Particularly in the case of BCPs with polyferrocenyldimethylsilane (PFS) as the core-forming block, micelle growth has many of the characteristics of living polymerization: the degree of supramolecular polymerization is controlled by the monomer (unimer) to initiator (seed) ratio, leading to rod-like micelles very uniform in length. Because the micelle ends are open to further growth, the micelles can be elongated by the addition of unimer, and if the newly added unimer has a chemically different corona-forming structure, block comicelles can be obtained. Thus sequential living CDSA represents a powerful approach to generating novel block structures. [26,27,39-42]

In contrast with the homopolymerization examples described above, copolymerization involves the simultaneous polymerization of two or more monomers. There are only rare reports of the co-assembly of low molecular weight unimers. An important example reported by Meijer, de Greef and coworkers involved chiral induction of helix formation by a mixture of *R*- and *S*-chiral enantiomers of oligo(p-phenylenevinylene) derivative. The co-assembly rate was highly dependent on the ratio between both chiral monomers.[43] Aida et al. found that the co-assembly of a racemic mixture of fluorinated chiral hexabenzocoronene on a common seed resulted in a tubular block structure. In their case, the helical senses of the newly formed block were solely determined by those of the helical seeds. However, they could not distinguish whether the block structure was an ABC triblock copolymer or a mixture of AB and AC diblock copolymers.[44] For CDSA of crystalline-coil BCPs, the copolymerization analog is the competitive addition to a growing micelle of two BCPs with a common crystallizable block. This situation can be achieved by feeding a blend of two BCPs to a seed solution. This co-assembly approach represents an alternative, more versatile, and simpler route to generating micelles with two or more chemically different corona chains.[45,46]

In 2010, we reported the co-assembly of two linear PFS-containing BCPs, PFS-*b*-polyisoprene (PFS-*b*-PI) and PFS-*b*-polydimethylsiloxane (PFS-*b*-PDMS) by seeded growth from a common micelle seed.[47] In this early study, we wished to examine how differences in corona composition and chain length affected the structure of the elongated

micelles formed. We found, for example, that the corona chains influence the packing density of BCP molecules in the micelles, as demonstrated by pronounced differences in the number of BCP molecules per nanometer; a property that we refer to as the linear aggregation number, $N_{agg,L}$. In spite of the large χ value for the PI and PDMS components ($\chi_{PI/PDMS}$ = 0.13 at 25 °C),[48] no evidence for corona chain segregation could be found by transmission electron microscopy (TEM), even after selectively staining the PI block with OsO_4.[47]

More recently we studied the co-assembly of a brush BCP and a linear BCP and examined how the steric bulk of the brush-like corona chains affected living CDSA behavior.[30] Starting with linear PFS_{68}-*b*-$PMVS_{670}$ (PMVS = polymethylvinylsiloxane, the subscripts refer to the mean number of monomer units), bottlebrush arms were created on PMVS block by a thiol-ene reaction with three different alklythiols (C_nH_{2n+1}-SH, n = 6, 12, 18, denoted BCP6, BCP12, and BCP18, respectively). The rate of micelle growth was retarded by the increasing length of alklythiols, and for BCP18, only a fraction of the unimers in solution added to the seed micelle. Since linear and brush BCPs added at different rates to the seed micelles, we examined the co-assembly behavior of the mixture of these two unimers. A fascinating morphology of tapered patches of $PMVS_{670}$ (visualized by OsO_4 staining) and the C_{18} brush (visualized by AFM) was observed. Co-assembly experiments of equimolar mixtures of PFS_{68}-*b*-$PMVS_{670}$ with BCP6 and BCP12 led to elongated micelles in which a gradient structure with patches of BCP12 could be visualized by OsO_4 staining, whereas no patches could be resolved in the experiment with BCP6. In order to explain the tapered structure of the micelles formed by co-assembly, we proposed a kinetic model in which the epitaxial addition rates of the different individual linear and brush BCPs combined with cumulative steric interactions of the brush block. The results indicate a preferential consumption of the linear BCP during the initial stage of micelle growth. As the linear unimer was consumed, the composition of the micelles changed in favor of brush BCP18, leading to a segmented, gradient comicelle architecture.

These examples suggest that the co-assembly of pairs of PFS BCPs with different corona chains has features in common with the living copolymerization of molecular monomers,[30,47]

where very similar reactivity ratios will lead to nearly random copolymers and differences in reactivity ratios can lead to the formation of blocky or gradient structures.[49] This idea opens the door to the construction of a broad variety of interesting and novel structures. While relatively little is known about reactivity ratios for the competitive assembly of pairs of core-crystalline polymers, the example of the co-assembly of PFS_{68}-*b*-$PMVS_{600}$ with BCP18 described above indicates that strongly cooperative effects are possible.[30]

We would like to explore simpler examples, involving the competitive co-assembly of pairs of linear PFS-containing BCPs. We choose examples in which we could selectively stain the corona chains of one of the BCPs. In this way we could use the micelle morphology as a qualitative measure of sequence distribution and compare competitive addition experiments with kinetic studies of micelle growth rates for the individual BCPs. Our working hypothesis was that similar growth rates of the two BCPs would lead to micelles with small surface patches due to microphase segregation of proximate corona chains along the cylindrical backbone. In contrast, we imagined that pronounced differences in the individual unimer addition rates to the growing micelles would lead to well-defined block co-micelles in which the individual blocks have spatially distinct coronas.

In this report, we describe experiments that examine competitive kinetics of living CDSA of pairs of PFS-containing linear BCPs in which the corona chains undergo spontaneous phase separation and no external staining is needed to see the patchy structure in TEM images. The polymers include PFS-*b*-PNIPAM and PFS-*b*-P2VP (PNIPAM = poly(N-isopropylacrylamide), P2VP = poly(2-vinlypridine)), as well as a lightly quaternized derivative of PFS-*b*-P2VP (PFS-*b*-$P2VP^{Q}$). We show that when the individual BCPs add at similar rates to seed micelles present in solution, one obtains patchy micelles characterized by small patches associated with local microphase segregation. When we changed the structure of one of the BCPs in a way that decreased the rate at which it adds epitaxially to the seed micelles, block comicelles were obtained. These results demonstrate the importance of growth kinetics in the co-assembly process and offer a simple method to tailor the micelle structure. The open ends of the patchy

micelles remained active for further growth, and in this way, multi-block co-micelles with patchy blocks and single-component (homo) blocks were obtained. The P2VP patches in these micelles could be decorated with either gold or platinum nanoparticles, yielding organic-inorganic hybrid material with potential application in catalysis.

2. RESULTS AND DISCUSSION

Coassembly experiments were carried out by the simultaneous addition of two PFS-containing BCPs as a concentrated solution in tetrahydrofuran (THF) to seed micelles in isopropanol (iPrOH). The seed micelles direct the living epitaxial growth of both unimers on their open termini (see experimental details in Supporting Information, SI).

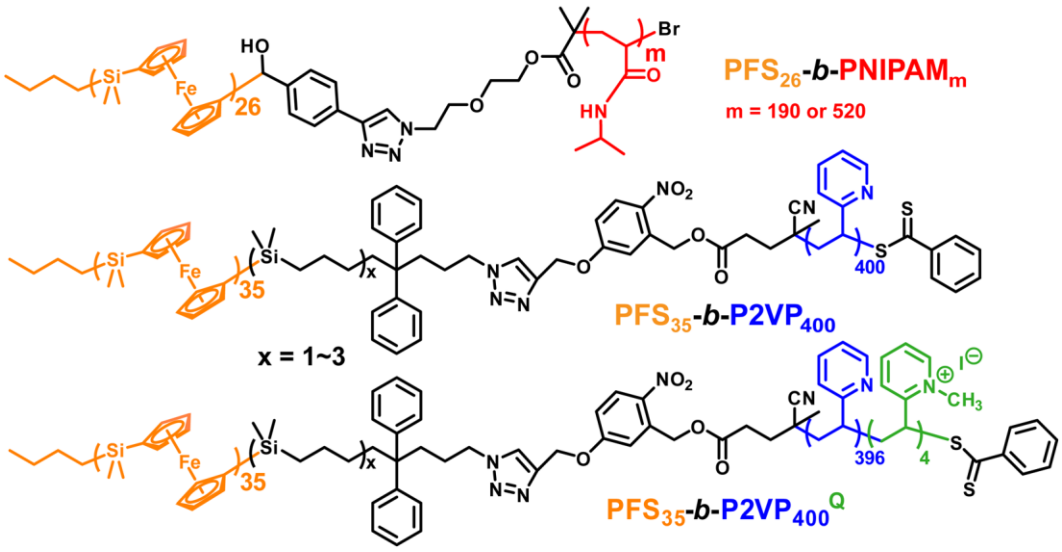

Chart 1. Structures of PFS-*b*-PNIPAM, PFS-*b*-P2VP, and PFS-*b*-P2VP^{Q} Diblock Copolymers. In the lower two structures, x takes a value of 1 to 3.[50]

2.1 Coassembly of PFS_{35}-b-$P2VP_{400}$ and PFS_{26}-b-$PNIPAM_{190}$

In our initial experiments, we examined the co-assembly of a 1:1 by weight mixture of PFS_{35}-*b*-$P2VP_{400}$ and PFS_{26}-*b*-$PNIPAM_{190}$ (Chart 1). Short micelle fragments of PFS_{35}-*b*-$P2VP_{400}$ (L_n = 40 ± 13 nm, L_w/L_n = 1.11, Figure S1 in SI) were employed as seeds. As shown in the TEM images Figure 1 and Figure S2, this led to elongated micelles, uniform in length as expected for seeded growth where no new nuclei form and all the added unimer grows

onto the seeds.[26,27] In addition, one can see that these micelles have a patchy texture (Figure 1a,d) in which the P2VP corona appears dark and the PNIPAM corona is hardly visible. The higher contrast for P2VP is related to its higher electron density. In some of the micelles, the central seed fragment can be distinguished, with tufts of P2VP domains apparent at various intervals along the micelle. Additional images at two different magnifications are presented in Figure S2-S3. Different patterns of patchy micelles are obtained if one uses an excess of one of the BCPs in the seeded growth experiment. A 3:1 mass ratio of PFS_{35}-*b*-$P2VP_{400}$ to PFS_{26}-*b*-$PNIPAM_{190}$ leads to the elongated micelles seen in Figure 1b,e and Figure S3a, with much thicker and denser coronas, reflecting the higher P2VP content. In contrast, micelles prepared from a 1:3 mass ratio of these two BCPs (Figure 1c,f and Figure S3c) appear much thinner. Aside from the thick dark patch indicating the location of the PFS_{35}-*b*-$P2VP_{400}$ seed, one sees only occasional patches of the P2VP corona along the micelle.

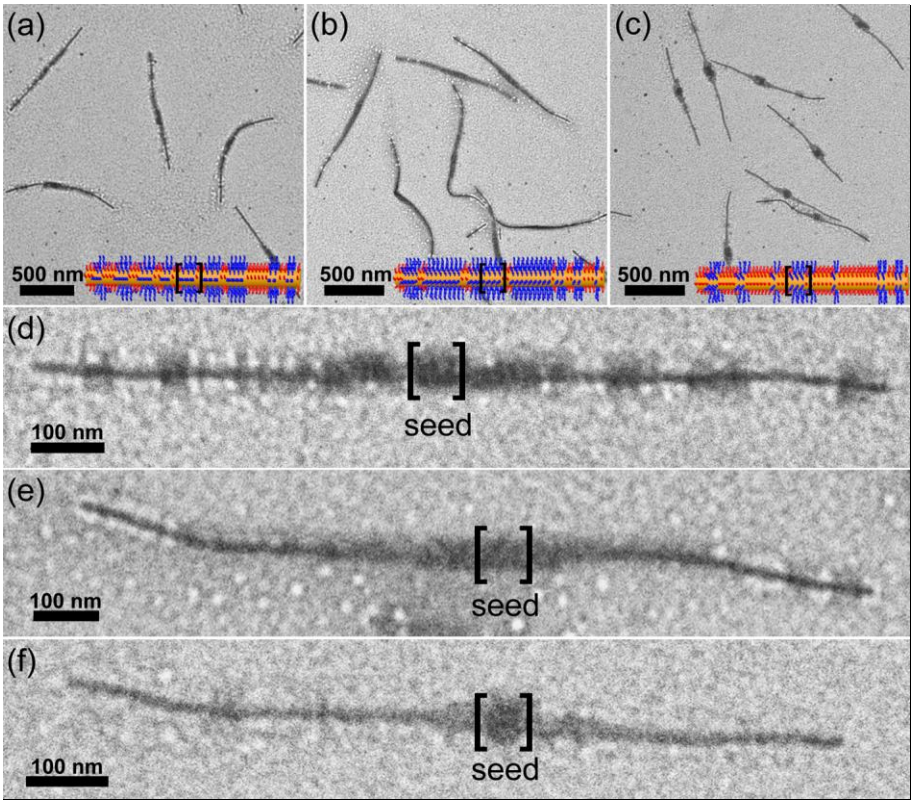

Figure 1. TEM images and corresponding schematic diagrams of the patchy micelles with segregated corona chains. The mass ratios of PFS_{35}-*b*-$P2VP_{400}$ to PFS_{26}-*b*-$PNIPAM_{190}$ are (a) and (d) 1:1, (b) and

(e) 3:1, (c) and (f) 1:3, respectively. (d), (e) and (f) are magnified TEM images of the micelles in (a), (b), and (c). The brackets indicate the position of PFS_{35}-*b*-$P2VP_{400}$ seeds. The yellow, blue, and red colors in the schematic diagrams indicate PFS, P2VP, and PNIPAM segments, respectively.

Another interesting feature of these co-assembled micelles became apparent when we controlled the molar ratio of the two BCPs. Here we found that the overall length of patchy micelles depended upon the composition of the unimer mixture. For example, their length increased as the fraction of PFS_{35}-*b*-$P2VP_{400}$ unimer in the mixture increased, even though the unimer-mixture-to-seed molar ratio remained constant (Figure S4). The overall length is a reflection of the way the BCP molecules pack in adding to the micelle, as measured by the linear aggregation number ($N_{agg,L}$), the number of BCP molecules per nm length of the micelles. We return to this topic in in **Section 2.5** below.

On a length scale of tens of nanometers, the structure of the micelles is a reflection of the order in which the two different BCPs added to the growing micelle. On a shorter length scale, structure can arise from phase segregation as the micelles dry on the grid. In order to understand the factors that can drive this demixing, we examine the Hansen solubility parameters of the two corona polymers. These values are collected in Table 1, where the total solubility parameter δ is calculated from the sum of squares of the individual dispersion δ_D, dipolar δ_P and hydrogen bonding components δ_H. The difference in total solubility parameters between PNIPAM (δ = 22.9 $MPa^{1/2}$) and P2VP (δ = 20.8 $MPa^{1/2}$) is larger than the difference in Hildebrand solubility parameters of PDMS (δ = 15.1 $MPa^{1/2}$) and PI (δ = 16.5 $MPa^{1/2}$),[51] for which no phase segregation could be detected in the comicelles formed by PFS-*b*-PDMS and PFS-*b*-PI.[47] Schmalz et al. observed patchy cylindrical micelles in the self-assembly of polystyrene-*b*-polyethylene-*b*-poly(methyl methacrylate) (PS-*b*-PE-*b*-PMMA) with a core-crystalline PE middle block.[32-35] The microphase separation between the PS and PMMA corona chains could be detected in spite of the very small solubility parameter difference between PS (δ = 18.6 $MPa^{1/2}$) and PMMA (δ = 18.3 $MPa^{1/2}$). They further confirmed the underlying coronal microphase separation in solution by using 2D ^{1}H nuclear Overhauser effect spectroscopy (NOESY).[32]

To examine this situation further, we calculate the Flory-Huggins interaction parameter between the corona chains ($\chi_{\text{PNIPAM-P2VP}}$) via eq 1.[52]

$$\chi_{\text{PNIPAM-P2VP}} = \frac{V_0}{RT}[(\delta_{\text{PNIPAM,D}} - \delta_{\text{P2VP,D}})^2 + 0.25(\delta_{\text{PNIPAM,P}} - \delta_{\text{P2VP,P}})^2 + 0.25(\delta_{\text{PNIPAM,H}} - \delta_{\text{P2VP,H}})^2] \quad (1)$$

Here V_0 is the geometric mean molar volume of the polymer segments (which are very similar), R is the gas constant, and T is the absolute temperature. In this way, we calculate $\chi_{\text{PNIPAM-P2VP}} \approx 1.0$ at 298 K. Based on the degree of polymerization of PNIPAM and P2VP, the critical value of χ (χ_{critical}) for phase separation in the bulk state can be calculated to be 0.0075 from eq 2,[53]

$$\chi_{critical} = \frac{1}{2}(N_{\text{PNIPAM}}^{-1/2} + N_{\text{P2VP}}^{-1/2})^2 \quad (2)$$

where N is the degree of polymerization of each corona block. The calculated $\chi_{\text{PNIPAM-P2VP}}$ is significantly higher than χ_{critical}, indicating the incompatibility between P2VP and PNIPAM and predicting that their mixture should phase separate.

Depending on the relative growth rates of the two BCP unimers and their concentrations, one might expect a gradient sequence along the cylinder axis. However, patchiness is mainly due to microphase separation of the two corona blocks. While it is possible that microphase separation occurs upon drying, we think that it is more likely that the patchy corona structure arises from an underlying microphase separation between P2VP and PNIPAM in solution, since their properties are quite different.

Table 1. Hansen solubility and molar volume of PNIPAM[54], P2VP[55], and iPrOH.[51]

Polymers	Molar Volume	Hansen Solubility Parameters ($MPa^{1/2}$)			
or Solvent	V (cm^3/mole)	δ_D	δ_P	δ_H	δ^a
PNIPAM	108.0	19.2	2.0	12.3	22.9
P2VP	107.8	17.9	8.8	5.9	20.8
iPrOH	76.6	15.8	6.1	16.4	23.6

a. $\delta^2 = \delta_D^2 + \delta_P^2 + \delta_H^2$

Several years ago, we reported the CDSA of a polystyrene-*arm*-polyisoprene-*arm*-polyferrocenylsilane (PS-*arm*-PI-*arm*-PFS) miktoarm star terpolymer, in which cylindrical micelles were formed with a PFS crystalline core and a segregated, patchy PS/PI corona.[31] In ABC triblock or star-like terpolymers with a crystallizable B block, the immiscible A and C blocks are covalently connected to the B block and thus are anchored at proximate locations along the cylindrical backbone. Therefore, both the A and the C blocks add to the growing micelle at the same time. Additionally, if one wants to modify the micelle structure, one has to synthesize new ABC BCPs, which is often very time-consuming.

In contrast, introducing blends of two linear PFS-containing BCP unimers into the seeded-growth process is a simple and effective approach for preparing patchy cylindrical micelles. Most importantly, one can use pairs of these BCPs to examine the competitive addition kinetics in the formation of cylindrical comicelles. One can imagine that the specific addition rate of a given BCP to an end of a growing micelle will depend upon its affinity for epitaxial attachment to the exposed PFS face of the micelle. Such growth is balanced by steric interactions of the soluble BCP chain with corona chains protruding from the growing end of the micelle. To explore this feature further, we compare the growth rate of the patchy comicelles with the growth rates of the corresponding single-component micelles.

2.2 Competitive Kinetics of Micelle Formation

The kinetics of micelle growth was studied by monitoring its length as a function of time after adding equimolar amounts of each unimer to the seed suspension (see experimental details in SI). First we investigated the growth rate of each individual BCP on the short seeds of PFS_{35}-*b*-$P2VP_{400}$. The increase in length as a function of time is presented in Figure S5 for PFS_{26}-*b*-$PNIPAM_{190}$ unimer and in Figure S6 for PFS_{35}-*b*-$P2VP_{400}$ unimer, accompanied by histograms of the length distribution that show that the distribution of lengths remains narrow. The growth rates are initially rapid, reaching 25 % to 40 % of the final length in ca. 10 min, but

then the growth rate slows substantially (Figure 2). The lengths appear to reach their final value after 7 days and remain almost the same after 80 to 110 days aging at 23 °C. Thus we assume that all of the unimers initially present in the solution have added onto the micelles.[26,27] Therefore, we use the lengths after aging these samples for 80 to 110 days as the final micelle length. The growth rate is defined as L_t/L_{final}, where L_t is the length increment of the micelle at time t, while L_{final} is the final length increment (total length - seed length, $L_{final} = L_{total} - L_{seed}$) determined after aging each sample. As shown in Figure 2, the growth rates of PFS_{35}-*b*-$P2VP_{400}$ and PFS_{26}-*b*-$PNIPAM_{190}$ are similar. When experiments were carried out with a mixture (1:1 molar ratio) of these two unimers, the micelle growth rate was almost identical (the TEM images used to construct this plot are presented in Figure S7). All of the three growth curves overlap well, indicating that both unimers have a nearly equal opportunity to grow on the ends of the seeds. While we have not attempted to fit these data to a kinetic model, we believe this similarity in growth rate for the two different unimers is likely critical for the formation of locally phase-separated patches as the elongation of micelles proceeds.

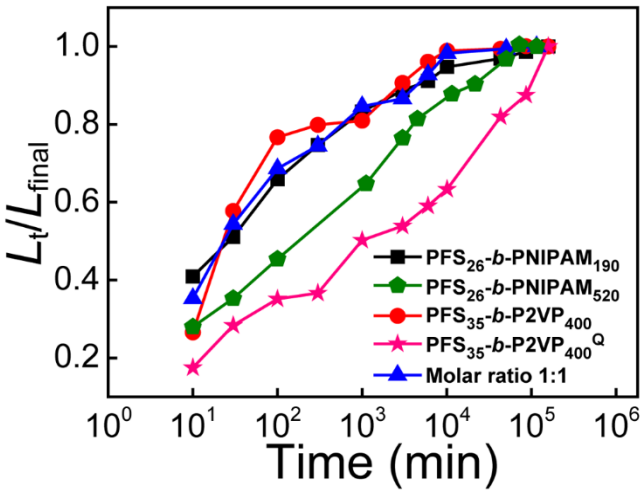

Figure 2. The growth kinetics plots of different unimers on PFS_{35}-*b*-$P2VP_{400}$ seeds. L_t is the length increment of the micelle at time t, while L_{final} is the final length increment (total length - seed length) after aging at least 80 days. Equimolar amounts of each unimer were injected to the diluted seed solution. Black squares: PFS_{26}-*b*-$PNIPAM_{190}$; Green pentagons: PFS_{26}-*b*-$PNIPAM_{520}$; Red circles: PFS_{35}-*b*-$P2VP_{400}$; Blue triangles: mixture of PFS_{26}-*b*-$PNIPAM_{190}$ and PFS_{35}-*b*-$P2VP_{400}$ (molar ratio 1:1). Note that for PFS_{35}-*b*-$P2VP_{400}^{Q}$, pink stars, the sample did not reach its final length after 110 days, and we arbitrarily set the length at that time as L_{total}.

Another more subtle feature of the competitive addition of the two BCPs to the seed micelle becomes apparent upon close inspection of the images of final micelles formed by the 1:1 mixture. Here it appears that the sizes of the patches are not uniformly distributed along the micelle. We used ImageJ to measure the P2VP patch size as a function of the distance from the central seed for all of the patches on 21 different micelles. The results are shown in Figure S8. While there is considerable scatter in the data, there is a trend to smaller P2VP patches as the distance from the seed increases from 50 nm to 600 nm. This can be attributed to the decrease of free PFS_{35}-*b*-$P2VP_{400}$ concentration in the solution during the epitaxial growth.

2.3 Kinetic Manipulation of the Micelle Formation

Decreasing the Growth Rate of PFS-b-P2VP by Quaternization (PFS_{35}-b-$P2VP_{400}^{Q}$). According to arguments presented in the previous section, if one type of unimer adds more rapidly to the ends of the growing micelle than the other in a simultaneous addition experiment, the final structure of the micelles formed should reflect this difference in addition rate. To test this idea, we took a sample of PFS_{35}-*b*-$P2VP_{400}$ and partially quaternized a small fraction of the pyridine groups with methyl iodide to obtain PFS_{35}-*b*-$P2VP_{400}^{Q}$. Based on previous work from our laboratory, we knew that even small extents of quaternization of PFS-*b*-P2VP significantly affected the morphology of the micelles.[56] Here we limited the extent of methylation of the pyridine groups to 1 mol % to ensure the solubility of the quaternized unimer PFS_{35}-*b*-$P2VP_{400}^{Q}$ in THF (see NMR in Figure S9). This corresponds to an average of about four $2VP^{Q}$ units per BCP chain. In a typical experiment, PFS_{35}-*b*-$P2VP_{400}^{Q}$ unimer was injected to a suspension of PFS_{35}-*b*-$P2VP_{400}$ seeds in iPrOH. TEM images of the micelles formed after various aging times as well as histograms of the micelle length are shown in Figure S10. Even after aging for 110 days, the average micelle length was only ca. 190 nm. The growth of the unimer could still be detected and these micelles did not reach their final length. Recall that for PFS_{35}-*b*-$P2VP_{400}$ itself, the micelles would have reached a length of ca. 470 nm in 7 days (Figure S6, SI). In order to compare the data for PFS_{35}-*b*-$P2VP_{400}^{Q}$ with that for PFS_{26}-*b*-$PNIPAM_{190}$ and PFS_{35}-*b*-$P2VP_{400}$, we arbitrarily set L_{final} = 190 nm to calculate an apparent growth rate. As seen in the bottom line

in Figure 2, this polymer added much more slowly to PFS_{35}-*b*-$P2VP_{400}$ seeds than the other two unimer samples.

To confirm the idea that corona modification was responsible for the striking decrease in growth rate, we carried out a second set of experiments in which we added an aliquot of PFS_{35}-*b*-$P2VP_{400}^{Q}$ in THF to seed micelles of PFS_{26}-$PNIPAM_{190}$ (L_n = 290 ± 76 nm, L_w/ L_n = 1.07, c.f., Figure S11) in iPrOH. Epitaxial growth in these CDSA experiments led to A'BA' triblock comicelles with PFS_{26}-*b*-$PNIPAM_{190}$ as the B block and PFS_{35}-*b*-$P2VP_{400}^{Q}$ as the A' block, reaching a length of ca. 500 nm over 45 days and ca. 520 nm after 80 days. TEM images and corresponding length histograms are presented in Figure S12. The results clearly show that this small extent of quaternization of PFS_{35}-*b*-$P2VP_{400}$ unimer significantly decreased its seeded-growth rate.

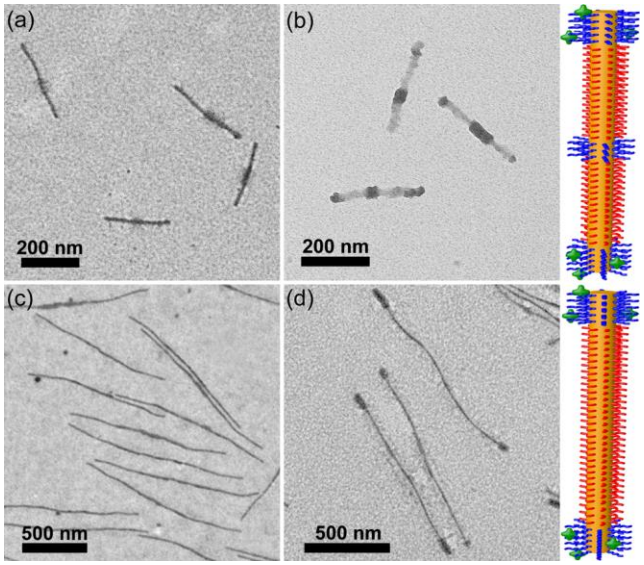

Figure 3. TEM images and corresponding schematic diagrams of the block comicelles obtained by adding the mixed unimers of PFS_{35}-*b*-$P2VP_{400}^{Q}$ and PFS_{26}-*b*-$PNIPAM_{190}$ (molar ratio 1:1) to (a)-(b) PFS_{35}-*b*-$P2VP_{400}$ seeds (L_n = 40 ± 13 nm), and (c)-(d) PFS_{26}-*b*-$PNIPAM_{190}$ seeds (L_n = 442 ± 59 nm), respectively. (a) and (c) show the micelles before staining by Karstedt's catalyst, while (b) and (d) show the micelles after staining. The yellow, blue, red, and green colors in the schematic diagrams indicate PFS, P2VP, PNIPAM, and positive charges, respectively.

We then carried out competition experiments in which we added a 1:1 (molar ratio) mixture of PFS_{35}-*b*-$P2VP_{400}^{Q}$ and PFS_{26}-*b*-$PNIPAM_{190}$ in THF to suspensions of seed micelles in iPrOH.

When we used 40 nm PFS_{35}-*b*-$P2VP_{400}$ seed micelles, block comicelles were obtained rather than patchy micelles (Figure 3a). To enhance the contrast, we treated the samples with Karstedt's catalyst (platinum(0)-1,3-divinyl-1,1,3,3-tetramethyldisiloxane complex) to stain the P2VP block and the P2VP component of the $P2VP^Q$ block with Pt NPs.[57,58] Figure 3b shows that the predominant structures are A'BABA' pentablock comicelles with PFS_{35}-$P2VP_{400}^Q$ end blocks (A') and a PFS_{35}-$P2VP_{400}$ center block (A). The length of the middle block (seed) is not obviously changed from that of the original seed micelles, suggesting that PFS_{35}-*b*-$P2VP_{400}^Q$ unimers seldom grow directly onto the seeds.

We also added the mixed unimers to the 442 nm PFS_{26}-*b*-$PNIPAM_{190}$ seeds. Here A'BA' triblock comicelles can be seen, particularly after staining with Pt NPs (Figure 3c-d). The length of the PFS_{26}-*b*-$PNIPAM_{190}$ B block increased from L_n = 442 nm to 1100 nm, whereas the length of the PFS_{35}-*b*-$P2VP_{400}^Q$ (A') block was only ca. 52 nm long. In Figure 3, we were unable to resolve PFS_{35}-*b*-$P2VP_{400}^Q$ domains in the elongated PFS_{26}-*b*-$PNIPAM_{190}$ B block even after staining. It is likely that some of PFS_{35}-*b*-$P2VP_{400}^Q$ unimers have been incorporated into the PFS_{26}-*b*-$PNIPAM_{190}$ blocks of the comicelles during the co-assembly. However, as a minor component in these blocks, they cannot be detected in the TEM images by staining. These results indicate that the growth rate of PFS_{26}-*b*-$PNIPAM_{190}$ unimer is much faster than that of PFS_{35}-*b*-$P2VP_{400}^Q$ unimer, and is consistent with the results of the individual kinetics experiments shown in Figure 2. These results confirm that one can take advantage of competitive kinetics in CDSA experiments to manipulate the structure of the elongated micelles that can be formed.

Decreasing the growth rate of PFS-b-PNIPAM by increasing PNIPAM length (PFS_{26}-b-$PNIPAM_{520}$). Previous experiments in our laboratory showed that the growth rate of PFS_{26}-*b*-$PNIPAM_{520}$ micelles in iPrOH was very slow.[59] This is likely due to the increase in solubility of the BCP and steric hindrance of the PNIPAM segment when its degree of polymerization is increased. Here we examined the seeded growth rate of PFS_{26}-*b*-$PNIPAM_{520}$ micelles onto 40 nm PFS_{35}-*b*-$P2VP_{400}$ seed micelles. TEM images and corresponding histograms

of the length distribution are presented in Figure S13. It takes more than 35 days for the micelles to reach their final length, and the time evolution of L_t/L_{final} is plotted in Figure 2. One can see that the growth rate for these single-component micelles is significantly slower than those for PFS_{26}-*b*-$PNIPAM_{190}$ or PFS_{35}-*b*-$P2VP_{400}$. We then carried out competition experiments adding a 1:1 (molar ratio) mixture of PFS_{26}-*b*-$PNIPAM_{520}$/PFS_{35}-*b*-$P2VP_{400}$ to the 40 nm PFS_{35}-*b*-$P2VP_{400}$ seed micelles.

As shown in Figure 4, only block comicelles rather than patchy comicelles can be observed. After selectively staining the PFS_{35}-*b*-$P2VP_{400}$ chains, we found the length of the seed block (dark segment in Figure 4b) increased from 40 nm to 210 nm. This result indicates that most of the PFS_{35}-$P2VP_{400}$ unimers added epitaxially onto the seeds and the growing micelles before PFS_{26}-*b*-$PNIPAM_{520}$ unimers added. After consumption of the PFS_{35}-*b*-$P2VP_{400}$, the growth of the PFS_{26}-*b*-$PNIPAM_{520}$ dominated the seeded-growth process, resulting in B'AB' triblock comicelles with PFS_{35}-$P2VP_{400}$ as the A block and PFS_{26}-$PNIPAM_{520}$ as the B' blocks. This experiment demonstrates that by choosing a BCP partner with a slower growth rate, for either component, block comicelles rather than patchy comicelles can be obtained. In other words, knowledge of the growth kinetics enables one to alter the growth sequence of the unimers. This method offers us a sophisticated strategy for controlling the morphology of the micelles obtained by the CDSA process.

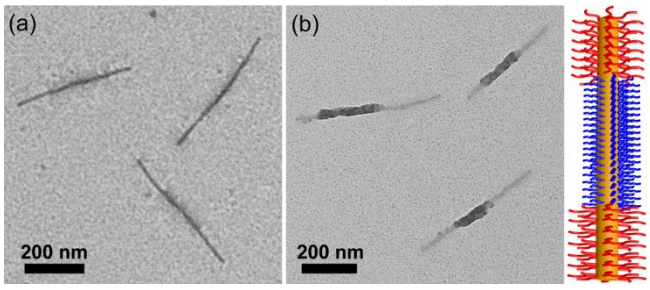

Figure 4. TEM images and corresponding schematic diagrams of the block comicelles (a) before and (b) after staining by Karstedt's catalyst. These micelles are obtained by adding the mixed unimers of PFS_{35}-*b*-$P2VP_{400}$ and PFS_{26}-*b*-$PNIPAM_{520}$ (molar ratio 1:1) to PFS_{35}-*b*-$P2VP_{400}$ seeds (L_n = 40 ± 13 nm). The yellow, blue, and red colors in the schematic diagrams indicate PFS, P2VP, and PNIPAM segments, respectively.

2.4 Controlling the Length and the Morphology of the Patchy Micelles

Since the seeded-growth of unimer in CDSA is a living process, the length of the cylindrical micelles can be controlled by varying the ratio of unimer to seed.[26,27] Here, this strategy is employed to control the length of patchy micelles. The PFS_{35}-*b*-$P2VP_{400}$ and PFS_{26}-*b*-$PNIPAM_{190}$ unimers were premixed (weight ratio 1:1) in THF to get a solution with c = 10 mg/mL. Then different amounts of unimer solution (up to 25 μL) were injected into the 40 nm PFS_{35}-*b*-$P2VP_{400}$ seed solution (0.005 mg/mL). As shown in Figure S14, patchy cylindrical micelles with uniform length can be obtained. The length of the micelles increases linearly as the increase of the mass ratio of unimer to seed. This living growth behavior is consistent with expectations based on a living CDSA process.[26,27]

We also have control of the overall morphology of these structures. For example, when longer PFS_{26}-*b*-$PNIPAM_{190}$ micelles (length: 442 nm) are employed as seeds for this unimer mixture, we obtain triblock comicelles with a single-component (homo) middle block and patchy end blocks (Figure 5a). If instead, we use as our seed structure a patchy micelle grown off a 40 nm PFS_{35}-*b*-$P2VP_{400}$ micelle fragments (c.f., Figure 1a) to direct the growth of PFS_{35}-*b*-$P2VP_{400}$ unimer, then we get triblock comicelles with patchy middle block and homo end blocks (Figure 5b). If the triblock comicelles shown in Figure 5a are employed as seeds, pentablock comicelles with patchy blocks and homoblocks can be obtained (Figure 5c). These experiments demonstrate the versatility of living CDSA in forming complex partially patchy structures with control over composition and length.

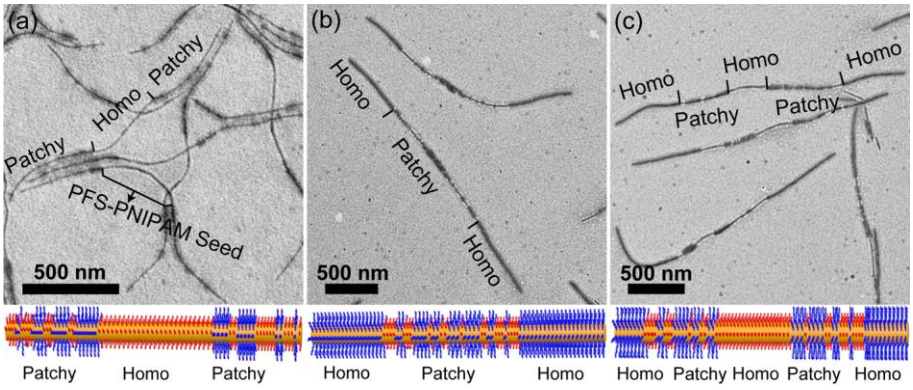

Figure 5. TEM images and corresponding schematic diagrams of (a) patchy-homo-patchy triblock comicelles, (b) homo-patchy-homo triblock comicelles, and (c) homo-patchy-homo-patchy-homo pentablock comicelles. The yellow, blue, and red colors in the schematic diagrams indicate PFS, P2VP, and PNIPAM segments, respectively.

2.5 The Linear Aggregation Number of the Patchy Cylindrical Micelles

As shown in Figure 1, and Figures S4-S6, we found that when equimolar amounts of unimers or unimer mixtures were added to aliquots of the same seed solution, the final lengths of the micelles were different. Increasing the mole fraction of PFS_{26}-*b*-$PNIPAM_{190}$ in the unimer mixture with PFS_{35}-*b*-$P2VP_{400}$ led to a decrease of the final length of the comicelles (Figure S4). Since each micelle contains on average the same number of BCP molecules, this difference must reflect differences in the packing density of BCPs in the micelle. A useful way to characterize this property is in terms of the linear aggregation number $N_{agg,L}$, which describes the number of BCP molecules per nm of micelle length. Since the overall aggregation number $N_{agg,L}$ of the PFS_{35}-*b*-$P2VP_{400}$ seed has been measured by laser light scattering (corresponding to $N_{agg,L,seed}$ = 2.0 molecules/nm),[60] we can calculate $N_{agg,L}$ values of the various micelles formed by seeded growth using eq 3.

$$N_{agg,L} = \left(\frac{m_{unimer1}}{M_{unimer1}} + \frac{m_{unimer2}}{M_{unimer2}}\right)\frac{M_{0,seed}}{m_{seed}}\frac{L_{seed,w}}{L_{final,n}}N_{agg,L,seed} \quad (3)$$

Here m_{unimer} is the mass of unimer, M_{unimer} is the molecular weight of unimer, $M_{0,seed}$ is the molecular weight of the BCP molecules in the seed, here PFS_{35}-*b*-$P2VP_{400}$, m_{seed} is the mass of seed, $L_{seed,w}$ is the weight average length of the seed, and $L_{final,n}$ is the number average length of the newly added block. This analysis assumes that all of the unimer added to the seed solution grows epitaxially onto the micelle seeds and that the micelles have reached their final length. The calculation details can be found in the SI and the results are shown in Figure 6 and in Table 2.

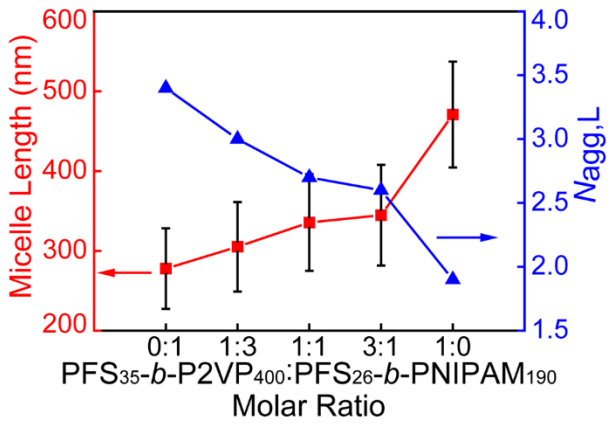

Figure 6. Plots of the comicelle length (red squares) and the linear aggregation number Nagg,L (blue triangles) versus the molar ratio of PFS_{35}-*b*-$P2VP_{400}$ to PFS_{26}-*b*-$PNIPAM_{190}$. Nagg,L values were calculated according to Eq 3.

The $N_{agg,L}$ value of the homomicelles (HM1) formed by growing PFS_{35}-*b*-$P2VP_{400}$ unimer on PFS_{35}-*b*-$P2VP_{400}$ seeds is calculated to be 1.9, which is very close to the value obtained by laser light scattering for the seed itself ($N_{agg,L,seed}$ = 2.0). As we have found previously, seeded growth of a single component micelle does not lead to a change in the number of BCPs per unit length. In contrast, we obtain a value of the $N_{agg,L}$ = 3.4 for the homomicelles (HM2) formed by growing PFS_{26}-*b*-$PNIPAM_{190}$ unimer on PFS_{35}-*b*-$P2VP_{400}$ seeds. The fact that the newly added block of HM2 is shorter than that of HM1, even though equimolar amounts of each were added to the seeds, can be explained by a larger number of BCP molecules per unit length for HM2. For the patchy comicelles, we find that the $N_{agg,L}$ decreased as the mole fraction of PFS_{35}-*b*-$P2VP_{400}$ was increased (Figure 6). Because of the difference in how the BCP molecules pack in the micelle core, the length of the patchy comicelles increased as the mole fraction of PFS_{35}-*b*-$P2VP_{400}$ in the unimer mixture increased.

This analysis helps us understand micelle lengths in the experiments with mixtures of unimers, but it does not tell us what structural features of the BCP determine the magnitude of $N_{agg,L}$.[61] In a previous publication, we reported that rod-like micelles of PFS_{26}-*b*-$PNIPAM_{520}$ were characterized by a very small value of $N_{agg,L}$ (ca. 1 BCP/nm).[59] The contrast with $N_{agg,L}$ = 3.4 for PFS_{26}-*b*-$PNIPAM_{190}$ indicates that corona repulsion for the polymer with the longer PNIPAM block must play an important role. It is also likely that the length of the PFS block is

also important.

Table 2. Characteristics of the seed micelles, homomicelles (HM), and patchy micelles (PM)

	m_{seed} (mg)	$10^{-15}\,N_{seed}$	$10^{-18}\,N_{unimer}$	$L_{total,n}$ (nm)[c]	$L_{total,w}$ (nm)[d]	$L_{total,w}/L_{total,n}$	$L_{final,n}$ (nm)[e]	$N_{agg,L}$
HM1[a]	0.02	2.70	2.17	471	480	1.02	431	1.9
HM2[a]	0.02	2.70	2.17	278	286	1.03	238	3.4
PM1[b]	0.02	2.70	2.17	345	356	1.03	305	2.6
PM2[b]	0.02	2.70	2.17	335	346	1.03	296	2.7
PM3[b]	0.02	2.70	2.17	305	315	1.03	265	3.0

a. HM1: Homomicelle blocks formed by growing PFS_{35}-*b*-$P2VP_{400}$ unimers on PFS_{35}-*b*-$P2VP_{400}$ seeds (Figure S6); HM2: Homomicelle blocks formed by growing PFS_{26}-*b*-$PNIPAM_{190}$ unimers on PFS_{35}-*b*-$P2VP_{400}$ seeds (Figure S5).

b. PM1, PM2, and PM3: Patchy micelles by growing mixed unimers on PFS_{35}-*b*-$P2VP_{400}$ seeds. The molar ratio of PFS_{26}-*b*-$PNIPAM_{190}$ to PFS_{35}-*b*-$P2VP_{400}$ are 1:3, 1:1, and 3:1, respectively (Figure S4).

c. $L_{total,n}$: number average micelle length at 110 days (or 80 days for PM1, PM2, and PM3)

d. $L_{total,w}$: weight average micelle length at 110 days (or 80 days for PM1, PM2, and PM3)

e. $L_{final,n} = L_{total,n} - L_{seed,n}$ (L_{seed} = 40 nm, $L_{seed,w}$ = 44 nm)

2.6 Loading of AuNP and PtNP to the Patchy Micelles

As reported by Schmalz, Greiner et al., cylindrical micelles with patchy coronas can be employed as carriers for metal nanoparticles (NPs) if the patches can be modified with appropriate functional groups to anchor the NPs.[62] These hybrid structures can be employed in heterogeneous catalysis.[63] In their experiments, they carried out an aminolysis reaction with *N*,*N*-dialkylethylenediamine on their PS-*b*-PE-*b*-PMMA triblock terpolymer to convert a fraction of the MMA groups to pendant tertiary amine groups. They were then able to load the PMMA-rich patches with gold nanoparticles (AuNPs). The patchy cylindrical micelles that we report in this paper have patches rich in P2VP and patches rich in PNIPAM, both of which are effective at binding AuNPs and PtNPs.[64]

We carried out these experiments on the patchy micelles shown in Figures 1a,d, prepared from a 1:1 (by weight) mixture of PFS_{35}-*b*-$P2VP_{400}$ and PFS_{26}-*b*-$PNIPAM_{190}$. To introduce gold

ions, a suspension of these micelles in iPrOH was treated with a solution of $HAuCl_4$, also in iPrOH. After successive sedimentation-redispersion cycles to remove excess $HAuCl_4$, AuNPs could be generated in two different ways. Treatment of the micelle solution with $NaBH_4$ led to formation of AuNPs *in situ*. Also, deposition on a TEM grid of the micelles to which Au ions were absorbed led to AuNP formation upon exposure to the electron beam. In Figure 7a and Figure S15a we show an image of a patchy micelle loaded with AuNPs after treatment with $NaBH_4$. The inset at higher magnification shows that discrete AuNPs (diameter: ~ 1.5 nm) are present in both P2VP and PNIPAM corona domains, but with a higher density in the P2VP-rich patches. The corona chains are very effective at preventing the aggregation and fusion of the NPs.

To introduce PtNPs, we treated the micelle suspension with Karstedt's catalyst plus 1,1,3,3-tetramethyldisiloxane (TMDS). PtNPs are formed *in situ* by the reduction of Karstedt's catalyst. We have used this approach in the past to introduce tiny PtNPs into the P2VP corona of block comicelles as a way of cross linking the corona chains.[57,58] As shown in Figure 7b and Figure S15b, this treatment leads to the PtNPs confined to the P2VP-rich patches of the micelles. The selective loading of PtNPs not only helps us to clearly distinguish the P2VP domains in the corona region by TEM, but it also does not perturb the PNIPAM domains. In solution, the solvent swollen PNIPAM chains can enhance the colloidal stability of the organic-inorganic hybrid micelles, facilitating potential applications in catalysis.

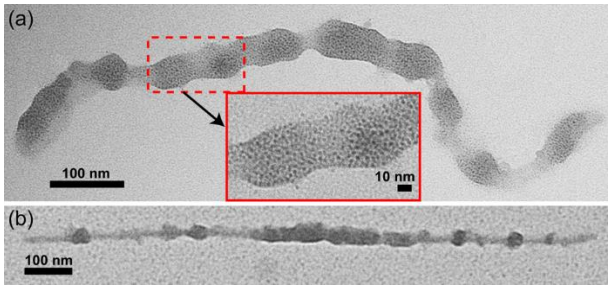

Figure 7. TEM images of the patchy comicelles loaded with (a) AuNPs and (b) PtNPs. The inset in (a) shows a magnified TEM image of the hybrid micelles. These hybrid structures were prepared using the patchy micelles shown in Figure 1a,d, in which a 1:1 (w/w) mixture of PFS_{35}-*b*-$P2VP_{400}$ and PFS_{26}-*b*-$PNIPAM_{190}$ were added to PFS_{35}-*b*-$P2VP_{400}$ seed micelles. Additional images and a brief discussion of the difference in shape of these metal-NP decorated micelles are presented in Figure S15.

3. CONCLUSION

We have examined a competitive kinetics approach to living crystallization-driven self-assembly, using pairs of PFS-containing BCPs with different corona-forming chains, as a way of generating both patchy micelles and block comicelles. This represents an example of living supramolecular chain copolymerization. In these seeded growth experiments, mixtures of two linear BCPs, PFS_{35}-*b*-$P2VP_{400}$ and PFS_{26}-*b*-$PNIPAM_{190}$, were added to PFS_{35}-*b*-$P2VP_{400}$ seed micelles. Both polymers added epitaxially at similar rates to the open ends of the growing micelles, leading to patchy micelles characterized by local microphase separation between the P2VP and PNIPAM chains. If however, the two PFS-containing BCPs in the mixture, examined separately, added to the seed micelles at very different rates, then this behavior carried over to the competitive kinetics experiment. The BCP with the faster addition rate was more effective in the initial addition to the seed micelles. As its unimer concentration in solution became depleted, the BCP with the slower intrinsic addition rate contributed to the micelle growth. If the difference in growth rate were large, then block comicelle-like structures were obtained.

The chemical structure of the polymer and the ratio of the lengths of the two blocks also affects how the BCPs pack in the core of the micelle, as reflected in the magnitude of $N_{agg,L}$, the number of BCP molecules per nm length of the micelle. Since the molecular weight and aggregation number are known for the PFS_{35}-*b*-$P2VP_{400}$ seed micelles used in many of these experiments, we were able to determine mean $N_{agg,L}$ values for a variety of different blend structures. If the $N_{agg,L}$ values of the individual BCP micelles are different, the mean $N_{agg,L}$ value in the blend structure is controlled by the molar ratio of the two unimers in the mixture.

These experiments raise the interesting question of what features of the PFS-containing BCP structures affect the rate at which they add to seed micelles in a living CDSA process. We show that a tiny extent of methylation (quaternization) of the 2VP groups of PFS_{35}-*b*-$P2VP_{400}$ (PFS_{35}-*b*-$P2VP_{400}^{Q}$) slows the growth rate substantially. Long corona-forming chains also slow the growth rate. Here we compare PFS_{26}-*b*-$PNIPAM_{190}$ with PFS_{26}-*b*-$PNIPAM_{520}$. It is also likely that the length of the PFS block and the block ratio of the PFS block compared to the

corona-forming block play important roles. These are issues that we hope to investigate in the future. Finally, we show that these patchy micelles can serve as effective hosts for AuNPs and PtNPs. For micelles with PNIPAM and P2VP patches in the corona, we show that AuNPs can locate in both domains, whereas the PtNPs can be selectively loaded in the P2VP domains. Such organic-inorganic hybrid cylindrical micelles can potentially be applied to heterogeneous catalysis.

ASSOCIATED CONTENT

Supporting Information Available:

Experimental details, kinetics study of the seeded-growth, additional figures (Figure S1-S15) of the patchy and block comicelles, NMR of PFS_{35}-*b*-$P2VP_{400}^{Q}$, and details about the $N_{agg,L}$ calculation. This material is available free of charge via the Internet at http://pubs.acs.org.

AUTHOR INFORMATION

Author Contribution

† J.X. and H.Z. contributed equally to this work

Corresponding Authors

* E-mail: mwinnik@chem.utoronto.ca (M.A.W.)

Notes

The authors declare no competing financial interest.

ACKNOWLEDGEMENTS

The Toronto authors thank NSERC Canada for their support of this research.

REFERENCES

(1) De Greef, T. F.; Smulders, M. M.; Wolffs, M.; Schenning, A. P.; Sijbesma, R. P.; Meijer, E. *Chem. Rev.* **2009**, *109*, 5687.

(2) Huang, Z.; Qin, B.; Chen, L.; Xu, J. F.; Faul, C. F.; Zhang, X. *Macromol. Rapid Commun.* **2017**, *38*, 1700312.

(3) Brunsveld, L.; Folmer, B.; Meijer, E. W.; Sijbesma, R. *Chem. Rev.* **2001**, *101*, 4071.

(4) Aida, T.; Meijer, E.; Stupp, S. *Science* **2012**, *335*, 813.

(5) Lutz, J.-F.; Lehn, J.-M.; Meijer, E.; Matyjaszewski, K. *Nat. Rev. Mater.* **2016**, *1*, 16024.

(6) de Greef, T. F.; Meijer, E. *Nature* **2008**, *453*, 171.

(7) Sorrenti, A.; Leira-Iglesias, J.; Markvoort, A. J.; de Greef, T. F.; Hermans, T. M. *Chem. Soc. Rev.* **2017**, *46*, 5476.

(8) Robinson, M. E.; Lunn, D. J.; Nazemi, A.; Whittell, G. R.; De Cola, L.; Manners, I. *Chem. Commun.* **2015**, *51*, 15921.

(9) Harada, A.; Takashima, Y.; Yamaguchi, H. *Chem. Soc. Rev.* **2009**, *38*, 875.

(10) Liu, Y.; Yu, Y.; Gao, J.; Wang, Z.; Zhang, X. *Angew. Chem., Int. Ed.* **2010**, *49*, 6576.

(11) Zheng, B.; Wang, F.; Dong, S.; Huang, F. *Chem. Soc. Rev.* **2012**, *41*, 1621.

(12) Li, S.-L.; Xiao, T.; Lin, C.; Wang, L. *Chem. Soc. Rev.* **2012**, *41*, 5950.

(13) Sun, R.; Xue, C.; Ma, X.; Gao, M.; Tian, H.; Li, Q. *J. Am. Chem. Soc.* **2013**, *135*, 5990.

(14) Zhang, W.; Jin, W.; Fukushima, T.; Saeki, A.; Seki, S.; Aida, T. *Science* **2011**, *334*, 340.

(15) Fenske, M. T.; Meyer-Zaika, W.; Korth, H.-G.; Vieker, H.; Turchanin, A.; Schmuck, C. *J. Am. Chem. Soc.* **2013**, *135*, 8342.

(16) Besenius, P. *J. Polym. Sci., Part A: Polym. Chem.* **2017**, *55*, 34.

(17) Robinson, M. E.; Nazemi, A.; Lunn, D. J.; Hayward, D. W.; Boott, C. E.; Hsiao, M.-S.; Harniman, R. L.; Davis, S. A.; Whittell, G. R.; Richardson, R. M.; De Cola, L.; Manners, I. *ACS Nano* **2017**, *11*, 9162.

(18) Mukhopadhyay, R. D.; Ajayaghosh, A. *Science* **2015**, *349*, 241.

(19) Kang, J.; Miyajima, D.; Mori, T.; Inoue, Y.; Itoh, Y.; Aida, T. *Science* **2015**, *347*, 646.

(20) Ogi, S.; Stepanenko, V.; Sugiyasu, K.; Takeuchi, M.; Würthner, F. *J. Am. Chem. Soc.* **2015**, *137*, 3300.

(21) Fukui, T.; Kawai, S.; Fujinuma, S.; Matsushita, Y.; Yasuda, T.; Sakurai, T.; Seki, S.; Takeuchi, M.; Sugiyasu, K. *Nat. Chem.* **2016**, *9*, 493.

(22) Ogi, S.; Sugiyasu, K.; Manna, S.; Samitsu, S.; Takeuchi, M. *Nat. Chem.* **2014**, *6*, 188.

(23) Guo, K.; Shillcock, J.; Lipowsky, R. *J. Chem. Phys.* **2009**, *131*, 015102.

(24) Schek, H. T.; Gardner, M. K.; Cheng, J.; Odde, D. J.; Hunt, A. J. *Curr. Biol.* **2007**, *17*, 1445.

(25) Schmelz, J.; Schacher, F. H.; Schmalz, H. *Soft Matter* **2013**, *9*, 2101.

(26) Wang, X.; Guerin, G.; Wang, H.; Wang, Y.; Manners, I.; Winnik, M. A. *Science* **2007**, *317*, 644.
(27) Gilroy, J. B.; Gädt, T.; Whittell, G. R.; Chabanne, L.; Mitchels, J. M.; Richardson, R. M.; Winnik, M. A.; Manners, I. *Nat. Chem.* **2010**, *2*, 566.
(28) Hailes, R. L.; Oliver, A. M.; Gwyther, J.; Whittell, G. R.; Manners, I. *Chem. Soc. Rev.* **2016**, *45*, 5358.
(29) He, W. N.; Xu, J. T. *Prog. Polym. Sci.* **2012**, *37*, 1350.
(30) Finnegan, J. R.; Lunn, D. J.; Gould, O. E. C.; Hudson, Z. M.; Whittell, G. R.; Winnik, M. A.; Manners, I. *J. Am. Chem. Soc.* **2014**, *136*, 13835.
(31) Nunns, A.; Whittell, G. R.; Winnik, M. A.; Manners, I. *Macromolecules* **2014**, *47*, 8420.
(32) Schmalz, H.; Schmelz, J.; Drechsler, M.; Yuan, J.; Walther, A.; Schweimer, K.; Mihut, A. M. *Macromolecules* **2008**, *41*, 3235.
(33) Schmelz, J.; Schmalz, H. *Polymer* **2012**, *53*, 4333.
(34) Schmelz, J.; Karg, M.; Hellweg, T.; Schmalz, H. *ACS Nano* **2011**, *5*, 9523.
(35) Schmelz, J.; Schedl, A. E.; Steinlein, C.; Manners, I.; Schmalz, H. *J. Am. Chem. Soc.* **2012**, *134*, 14217.
(36) Inam, M.; Cambridge, G.; Pitto-Barry, A.; Laker, Z. P.; Wilson, N. R.; Mathers, R. T.; Dove, A. P.; O'Reilly, R. K. *Chem. Sci.* **2017**, *8*, 4223.
(37) Arno, M. C.; Inam, M.; Coe, Z.; Cambridge, G.; Macdougall, L. J.; Keogh, R.; Dove, A. P.; O'Reilly, R. K. *J. Am. Chem. Soc.* **2017**, *139*, 16980.
(38) Petzetakis, N.; Dove, A. P.; O'Reilly, R. K. *Chem. Sci.* **2011**, *2*, 955.
(39) Boott, C. E.; Gwyther, J.; Harniman, R. L.; Hayward, D. W.; Manners, I. *Nat. Chem.* **2017**, *9*, 785.
(40) Gädt, T.; Ieong, N. S.; Cambridge, G.; Winnik, M. A.; Manners, I. *Nat. Mater.* **2009**, *8*, 144.
(41) Qiu, H.; Hudson, Z. M.; Winnik, M. A.; Manners, I. *Science* **2015**, *347*, 1329.
(42) Rupar, P. A.; Chabanne, L.; Winnik, M. A.; Manners, I. *Science* **2012**, *337*, 559.
(43) Korevaar, P. A.; Grenier, C.; Markvoort, A. J.; Schenning, A. P.; de Greef, T. F.; Meijer, E. *Proc. Natl. Acad. Sci. U.S.A* **2013**, *110*, 17205.
(44) Zhang, W.; Jin, W.; Fukushima, T.; Mori, T.; Aida, T. *J. Am. Chem. Soc.* **2015**, *137*, 13792.
(45) Zhu, J.; Zhang, S.; Zhang, K.; Wang, X.; Mays, J. W.; Wooley, K. L.; Pochan, D. J. *Nat. Commun.* **2013**, *4*, 2297.
(46) Pochan, D. J.; Zhu, J.; Zhang, K.; Wooley, K. L.; Miesch, C.; Emrick, T. *Soft Matter* **2011**, *7*, 2500.
(47) Cambridge, G.; Guerin, G.; Manners, I.; Winnik, M. A. *Macromol. Rapid Commun.* **2010**, *31*, 934.
(48) Cochran, E. W.; Morse, D. C.; Bates, F. S. *Macromolecules* **2003**, *36*, 782.

(49) Odian, G. *Principles of Polymerization, 4th ed.; John Wiley & Sons, Inc.: Hoboken, NJ, 2004.*
(50) Kloninger, C.; Rehahn, M. *Macromolecules* **2004**, *37*, 1720.
(51) Brandrup, J.; Immergut, E. H.; Grulke, E. A. *Polymer Handbook; Wiley: New York, 1999; Section VII, 675-714.*
(52) Hansen, C. M. *Hansen Solubility Parameters: A User's Handbook. CRC Press: U.S.A, 2000*.
(53) Rubinstein, M.; Colby, R. H. *Polymer Physics; Oxford University Press: New York 2003*.
(54) Ahmad, H. *J. Macromol. Sci., Part A: Chem.* **1982**, *17*, 585.
(55) Geldhauser, T.; Walheim, S.; Schimmel, T.; Leiderer, P.; Boneberg, J. *Macromolecules* **2010**, *43*, 1124.
(56) Gonzalez-Alvarez, M. J.; Jia, L.; Guerin, G.; Kim, K. S.; An Du, V.; Walker, G.; Manners, I.; Winnik, M. A. *Macromolecules* **2016**, *49*, 7975.
(57) Qiu, H.; Gao, Y.; Boott, C. E.; Gould, O. E.; Harniman, R. L.; Miles, M. J.; Webb, S. E.; Winnik, M. A.; Manners, I. *Science* **2016**, *352*, 697.
(58) Wang, H.; Wang, X.; Winnik, M. A.; Manners, I. *J. Am. Chem. Soc.* **2008**, *130*, 12921.
(59) Zhou, H.; Lu, Y.; Zhang, M.; Guerin, G.; Manners, I.; Winnik, M. A. *Macromolecules* **2016**, *49*, 4265.
(60) Zhou, H.; Lu, Y.; Qiu, H.; Guerin, G.; Manners, I.; Winnik, M. A. *Macromolecules* **2015**, *48*, 2254.
(61) Guerin, G.; Rupar, P.; Molev, G.; Manners, I.; Jinnai, H.; Winnik, M. A. *Macromolecules* **2016**, *49*, 7004.
(62) Schöbel, J.; Karg, M.; Rosenbach, D.; Krauss, G.; Greiner, A.; Schmalz, H. *Macromolecules* **2016**, *49*, 2761.
(63) Schöbel, J.; Burgard, M.; Hils, C.; Dersch, R.; Dulle, M.; Volk, K.; Karg, M.; Greiner, A.; Schmalz, H. *Angew. Chem., Int. Ed.* **2017**, *56*, 405.
(64) Nguyen, H. H.; Payré, B.; Fitremann, J.; Lauth-de Viguerie, N.; Marty, J.-D. *Langmuir* **2015**, *31*, 4761.

For Table of Content Use Only

Title: Competitive Self-Assembly Kinetics as a Route to Controlling the Morphology of Core-Crystalline Cylindrical Micelles

Authors: Jiangping Xu, Hang Zhou, Qing Yu, Ian Manners, and Mitchell A. Winnik

TOC Figure